Cerebral Cortex, November 2021;31: 5225–5238

https://doi.org/10.1093/cercor/bhab153
Advance Access Publication Date: 6 July 2021
Original Article

ORIGINAL ARTICLE

Interstitial Axon Collaterals of Callosal Neurons Form Association Projections from the Primary Somatosensory to Motor Cortex in Mice

Yuichiro Oka[1,2,5,6], Miyuki Doi[1], Manabu Taniguchi[1], Sheena Y. X. Tiong[1,2,4], Hisanori Akiyama[1], Takuto Yamamoto[1], Tokuichi Iguchi[1,5,7] and Makoto Sato[1,2,3,5,6]

[1]Department of Anatomy and Neuroscience, Graduate School of Medicine, Osaka University, Suita, Osaka 565-0871, Japan, [2]Molecular Brain Science, Division of Developmental Neuroscience, Department of Child Development, United Graduate School of Child Development, Osaka University, Kanazawa University, Hamamatsu University School of Medicine, Chiba University, and University of Fukui (UGSCD), Osaka University, Suita, Osaka 565-0871, Japan, [3]Graduate School of Frontier Biosciences, Osaka University, Suita, Osaka 565-0871, Japan, [4]Institute of Biological Sciences, Faculty of Science, University of Malaya, Kuala Lumpur 50603, Malaysia, [5]Division of Cell Biology and Neuroscience, Department of Morphological and Physiological Sciences, Faculty of Medical Sciences, University of Fukui, Eiheiji, Fukui 910-1193, Japan, [6]Research Center for Child Mental Development, University of Fukui, Eiheiji, Fukui 910-1193, Japan and [7]Present address: Department of Nursing, Faculty of Health Science, Fukui Health Science University, Fukui, Fukui 910-3190, Japan

Address correspondence to Makoto Sato, Department of Anatomy and Neuroscience, Graduate School of Medicine, Osaka University, 2-2 Yamadaoka, Suita, Osaka 565-0871, Japan. E-mail: makosato@anat2.med.osaka-u.ac.jp

Abstract

Association projections from cortical pyramidal neurons connect disparate intrahemispheric cortical areas, which are implicated in higher cortical functions. The underlying developmental processes of these association projections, especially the initial phase before reaching the target areas, remain unknown. To visualize developing axons of individual neurons with association projections in the mouse neocortex, we devised a sparse labeling method that combined *in utero* electroporation and confocal imaging of flattened and optically cleared cortices. Using the promoter of an established callosal neuron marker gene that was expressed in over 80% of L2/3 neurons in the primary somatosensory cortex (S1) that project to the primary motor cortex (M1), we found that an association projection of a single neuron was the longest among the interstitial collaterals that branched out in L5 from the earlier-extended callosal projection. Collaterals to M1 elongated primarily within the cortical gray matter with little branching before reaching the target. Our results suggest that dual-projection neurons in S1 make a significant fraction of the association projections to M1, supporting the directed guidance mechanism in long-range corticocortical circuit formation over random projections followed by specific pruning.

Key words: barrel cortex, corticocortical projection, inter-areal connection, optical tissue clearing, sensorimotor integration

Introduction

Information processing units underlie the functional areas dividing tangential neocortical expanse. Direct neuronal projections (association projections) interconnect distant regions in the ipsilateral hemisphere, which likely forms the foundation of higher cortical functions particularly in primates including humans (Sousa et al. 2017). Impairments in these projections are associated with neurodevelopmental and psychological disorders (Jou et al. 2011; Katz et al. 2016; Chiang et al. 2017; Thompson et al. 2017; Fitzgerald et al. 2018). Among the six layers of the neocortex, upper layer (supragranular layers; layers II and III in humans and L2/3 in rodents) neurons are a major source of axons that form association projections (Jones and Wise 1977; Greig et al. 2013). These findings suggest that the enormous increase in upper layer neurons in humans and apes (Marin-Padilla 1978; Rockel et al. 1980; Hutsler et al. 2005) underlies the thickening of the projection tracts, which possibly gives rise to higher cognitive functions.

Association projections can have either a "feedforward" or a "feedback" nature; "feedforward" projections originate in the primary sensory areas and extend to higher order sensory and association areas and "feedback" projections occur in the opposite direction (Felleman et al. 1991; Coogan and Burkhalter 1993; Scannell et al. 1995). The terminal organization of these projections exhibits a columnar structure spanning the cortical height, which is a conserved feature among primates and rodents (Goldman and Nauta 1977; Isseroff et al. 1984) and is important for integrative processing by postsynaptic neurons (Takahashi et al. 2016; Fletcher and Williams 2019). Topographic projection patterns exist in both feedforward and feedback projections (Mao et al. 2011; Han et al. 2018; Minamisawa et al. 2018). A recent study showed that a clonally related and synaptically connected group of neurons in the mouse primary somatosensory cortex (S1) project to a neuronal population in the primary motor cortex (M1) that are clonally related to each other, and vice versa (Ren et al. 2019). However, it remains elusive how such connection patterns are established during development.

The developmental processes of association projections have been studied mainly in primates, carnivores, and rodents. Retrograde tracing from target areas revealed postnatal reaching of association projections that originate from an ipsilateral area, in contrast to early, prenatal reaching of callosal projections (Mitchell and Macklis 2005). Anterograde tracing of developing association projections suggests a two-step model for projection growth: initial random extension of axonal branches to regions larger than the final target area, followed by selective eliminations leaving specific connections (Price and Blakemore 1985; Callaway and Katz 1990). Despite the significant contributions of prior studies to understanding the developmental process of association projections, both approaches have limitations. In principle, retrograde tracing cannot examine the behaviors of developing axons prior to reaching their target, whereas classic anterograde tracing only specifies the areas where the neurons reside. Recent techniques using Cre-driver mouse lines and recombination-dependent reporter-expressing adeno-associated viruses (AAVs) have largely overcome this problem, but these techniques are still not ideal when applied at early postnatal stages, given their temporal requirement for protein expression after viral injection.

Here, we studied the developmental processes of axon projection at a single-neuron resolution, focusing on the initial phase of association projection formation, the phase until the target is reached. Our novel sparse labeling method of developing cortical neurons employed *in utero* electroporation (IUE) with a Cre-driver under the promoter of a gene that was expressed in a large fraction of layer 2/3 neurons that made association projections from S1 to M1. We found that association projection in the mouse neocortex arose as the longest collateral of a "dual-projection" neuron, projecting to both ipsilateral and contralateral targets. The longest collateral extended without branching until reaching its target area and it was significantly longer than the other collaterals in the initial phase of circuit formation.

Materials and Methods

Animals

All animal experiments were approved by the Animal Research Committee of University of Fukui and the Animal Experimentation Committee of Osaka University, and were performed in accordance with the Regulations for Animal Research at University of Fukui and the Regulations on Animal Experimentation at Osaka University. ICR mice were purchased from Japan SLC Inc. and kept under 12-h/12-h light/dark cycle. They were allowed to feed and drink ad libitum. Three-week-old postnatal day 21 (P21) mice were used for tracing experiments and quantifications. Both male and female embryos at embryonic day 15.5 (E15.5) were used for IUE. Pups at P3, P5, and P7 were used for tissue processing and imaging. Pups at P10 and P29 were used for double labeling with *in situ* hybridization (ISH) and immunohistochemistry. Pups at P5 were used for double immunohistochemistry. The day a vaginal plug was detected was designated as E0.5. The day of birth was designated as P0.

Retrograde Tracing

P21 mice were intraperitoneally injected with a combination anesthetic (MMB: 0.3 mg/kg medetomidine, 4.0 mg/kg midazolam, and 5.0 mg/kg butorphanol). After the pedal withdrawal reflex disappeared, the mice were placed in the stereotaxic apparatus (Narishige), and the scalp and skull were opened. Green Retrobeads™ [GRB; Lumafluor; 1:1 dilution with phosphate-buffered saline (PBS)] or 4% FluoroGold (FluoroGold™, Fluorochrome; FG) in water, both containing 1 mg/mL Fast Green, was pressure-injected using a pulled and sharpened glass capillary needle (30–40 μm of outer diameter) connected to a Hamilton syringe via a connecting tube. The injection coordinates were determined according to the adult mouse brain atlas (Franklin and Paxinos 2008): (2.0 mm anterior to bregma, 1.5 mm lateral, 0.5 mm below the pial surface) and (1.5 mm, 1.5 mm, 0.5 mm) for M1 on the right hemisphere and (0.5 mm posterior to bregma, 3.0 mm lateral, 0.5 mm below the pial surface), (1.0 mm, 3.0 mm, 0.5 mm), (1.0 mm, 3.5 mm, 0.5 mm), (1.5 mm, 2.5 mm, 0.5 mm), (1.5 mm, 3.0 mm, 0.5 mm), (1.5 mm, 3.5 mm, 0.5 mm), and (2.0 mm, 3.0 mm, 0.5 mm) for contralateral S1 on the left hemisphere. The injection volume at each site was 30–40 nL. After suturing and recovery from anesthesia, mice were given a recovery time of 4–8 days. For tracing with GRB, the brains were dissected out and coronal sections were cut with a vibratome (LinearSlicer PRO7, Dosaka EM) and stained with Hoechst.

In situ Hybridization (ISH) and Immunohistochemistry

For ISH, mice at P1, P3, P5, and P29 were anesthetized by hyperthermia (for P1, P3, and P5) or intraperitoneal injection of MMB

(P29), and perfused first with ice-cooled PBS and then with 4% paraformaldehyde (PFA) in PBS. Brains were dissected out and fixed in 4% PFA in PBS at 4 °C overnight, cryoprotected in 30% sucrose in PBS at 4 °C overnight, and then embedded in Tissue-Teck® O.C.T. compound (Sakura). Cryostat sections (16 µm-thick) were thaw-mounted onto SuperFrost® glass slides (Matsunami) and stored at −80 °C until use. Sections were dried immediately with a hair dryer for at least 1 h before being subjected to ISH. ISH with the *Plxnd1* probe was performed as described previously (Yagi et al. 2016), except that proteinase K digestion was performed at a half concentration for 5 min for the P1, P3, and P5 samples.

For double labeling with retrograde tracing, brain sections from FG-injected mice were subjected to hybridization with the *Plxnd1* probe. After stringent washing, sections were incubated with sheep anti-DIG Fab fragment conjugated with alkaline phosphatase (Roche; 1:1000) and a rabbit anti-FG antibody (AB153, Millipore; 1:1000) at room temperature for 2 h. Anti-DIG binding was detected with NBT/BCIP. After adequate signal development, sections were mounted with PBS for imaging with a BX50 microscope (Olympus) equipped with the DP71 camera (Olympus) (ISH only images). Subsequently, sections were rinsed in PBS and anti-FG binding was detected with signal amplification using an Elite ABC Rabbit IgG kit (Vector) and DAB detection kit (Vector). Stained sections were mounted with Fluoromount™ (Diagnostic BioSystems) and imaged with the BX50 equipped with the DP71 camera and the BZ-X700 microscope (Keyence) (ISH + IHC images).

For double labeling with immunohistochemistry against GFP, coronal brain sections from P10 and P29 mice electroporated with pPlxnd1-Cre (see below) and pCALNL-GFP [generous gifts from C. Cepko (Addgene #13770; Matsuda and Cepko 2007)] were subjected to hybridization with the *Plxnd1* probe. Probe hybridization was detected with the sheep anti-DIG Fab fragment conjugated with peroxidase (Roche; 1:100) and GFP was detected with chicken anti-GFP antibody (ab13970, Abcam; 1:1000). Anti-DIG binding was detected with the TSA Biotin System (Perkin Elmer) and streptavidin-conjugated Alexa Fluor 564® (Invitrogen; 1:200). Anti-GFP binding was detected with goat anti-chicken IgY conjugated with Alexa Fluor 488 (Invitrogen; 1:200). Sections were counterstained with DAPI (Dojindo; 1:1000). Stained sections were mounted with Fluoromount™ and imaged under the LSM880 with Airyscan (Leica).

For double labeling immunohistochemistry with GFP and SATB2, coronal brain sections from P5 mice electroporated with pPlxnd1-Cre and pCA-mTmG [generous gifts from L. Luo (Addgene # 26123; Muzumdar et al. 2007)] were reacted with chicken anti-GFP antibody and mouse anti-SATB2 (ab51502, Abcam, 1:200). Specific binding was detected with the donkey anti-chicken IgY conjugated with Alexa Fluor® 488 (Jackson, 1:200) and the donkey anti-mouse IgG conjugated with CF® 633 (Biotium, 1:200). Sections were counterstained with DAPI. Stained sections were mounted with Fluoromount™ and imaged under the LSM880 with Airyscan (Leica).

Plasmid Constructs

Tα-Cre was a generous gift from T. Miyata (Sakakibara et al. 2014). The BAC clone (BX2707) containing the *Plxnd1* gene locus with the *Cre* gene inserted at the translation start site was purchased from BACPAC Resources Center. The 16.4 kb genomic DNA fragment upstream from the translation start site together with the *Cre* gene was retrieved by homologous recombination in *E. coli*. The retrieving vector pKan was our original minimal vector carrying a ColE1 replication origin, the kanamycin resistance gene, and a multiple cloning site (MCS) with *Kpn*I, *Not*I, *Pme*I, and *Sal*I restriction sites. This vector fragment was amplified from pEGFP-C1 (Clontech) by PCR using a primer pair appended with restriction sites (*Not*I-*Kpn*I-Kan-fw, 5′-AAACGCGGCCGCGGTACCCAGGCAGAAGTATGCAAAGC-3′ and *Pme*I-*Sal*I-ColE-rv, 5′-AAACGTCGACAGGCCAGGAACCGTAA-AAAG-3′). The 5′- and 3′ -homology arms (HAs) were PCR-amplified from the BAC clone with primer pairs appended with restriction sites (*Not*I-5′-HA-fw, 5′-AAAAAGCGGCCGCGTCTCCAG GGTCTTGGTTGA-3′; *Eco*RV 5′-HA-rv, 5′-AAAAAGATATCGGGATTT AGCTCAGGGGTA-3′; *Eco*RV-3′-HA-fw, 5′-AAAAAGATATCCACCG TGTACTTGGCGGCAGTGA-3′; and *Sal*I-3′-HA-rv, 5′-AAAAAGTCGA CTGGCACTCGACAGTTGGTAC-3′). The amplified fragments were first cloned into the pGEM-T vector (Promega), and then excised with the respective restriction enzymes. Both HAs were simultaneously ligated into pKan at its *Not*I and *Sal*I sites, resulting in pKan-53HAs. Homologous recombination was performed in the DH10B strain of *E. coli* using a BAC Subcloning Kit with pRed/ET (Gene Bridge GmbH) following the manufacturer's instructions, except that the pKan-53HAs vector linearized with *Eco*RV and dephosphorylated was used instead of the minimal vector provided by the manufacturer. The retrieved plasmid was named pPlxnd1-Cre.

Cre-Dependent Cre Expression Vector, pCAGGS-DIO-iCre

The pCAGGS vector (Niwa et al. 1991) was modified to obtain pCAGGS-5MCS that carried a new MCS (*Bgl*II, *Not*I, *Eco*RI, *Eco*RV, and *Xho*I). A *Bgl*II-loxP-lox2272-*Not*I fragment was PCR-amplified with a primer pair (*Bgl*II-loxpLOX2272-fw, 5′-ACCAGATCTataacttcgtatagcatacattatacgaagttatATAACTTCGTAT AGGATACT-3′ and *Not*I-LOX2272loxp-rv, 5′-cggGCGGCCGCATAAC TTCGTATAAAGTATCCTATACGAAGTTATataacttcgtataatgtatg-3′) and cloned into pCAGGS-5MCS digested with *Bgl*II and *Not*I to obtain pCAGGS-loxP-lox2272. An iCre-WPRE fragment was excised from paavCAG-iCre (generous gift from J. Kim, Addgene # 51904; Druckmann et al. 2014) with *Not*I and *Bam*HI. A *Bam*HI-cloxP-clox2272-*Xho*I fragment was PCR-amplified with a primer pair (*Bam*HI-cloxpcLOX2272-fw, 5′-GGTG*GATCC*ataacttcgtataatgtatgctatacgaagttatATAACTTCGTAT AAAGTATC-3′ and *Xho*I-cLOX2272cloxp-rv, 5′-TCA*CTCGAG*ATAAC TTCGTATAGGATACTTTATACGAAGTTATataacttcgtatagcataca-3′). These fragments were simultaneously cloned into pCAGGS-loxP-lox2272 digested with *Not*I and *Xho*I to obtain pCAGGS-DIO-iCre. Using the Stbl4 strain of *E. coli* and culturing at low temperature (20 °C) with tetracycline were crucial to minimize unwanted recombination in the bacteria that would otherwise occur in normal culture conditions.

In utero Electroporation (IUE)

Plasmids were introduced into cortical neurons in the ventricular zone by IUE using a previously described method (Iguchi et al. 2012) with some modifications. In brief, on E15.5, pregnant ICR female mice were anesthetized by intraperitoneal injection of MMB. Approximately 0.5 µL of plasmids (up to 2.5 µg/µL in total) was injected into the lateral ventricle of embryos. The ratio of plasmids used was pPlxnd1-Cre: pCALNL-GFP = 1:2000 (Fig. 2), pPlxnd1-Cre: pCA-mTmG = 1:2000 (Fig. 3),

Tα-Cre: pCA-mTmG: pCAGGS-DIO-iCre = 1:2000:20 (Fig. 5), and pPlxnd1-Cre: pCA-mTmG: pCAGGS-DIO-iCre = 1:2000:20 (Figs 6, 7A, Supplementary Figures S3, S4, and S5). Five cycles of square electric pulses (35 V, 50 ms) at 1 Hz were delivered. After suturing and recovery, the mice were kept until pups were used. It should be noted that we could not exclude the possibility that the GFP-labeled neurons at P3, P5, and P7 represented largely overlapping but distinct populations, as the expression level of *Plxnd1* in layer 2/3 increased from the early postnatal stage (P1–5, Fig. 4) to the juvenile stage (P29, Fig. 1).

Flat-Mount Preparation of Cortices

Electroporated pups were perfused with ice-cooled PBS followed by 4% PFA in PBS and the brains were dissected out. Cortices together with the white matter were removed from the rest of the telencephalon, and flattened between two siliconized coverslips with 1.5-mm-thick silicone rubber pieces (Togawa rubber Co., Ltd) as spacers. Coverslips were held with black metal binder clips on both ends, and the whole preparation was soaked in 4% PFA in PBS at 4 °C for 3 days for postfixation. Samples were kept in PBS at 4 °C until use.

Optical Clearing

Optical clearing of flat-mounted cortices from P3 and P5 brains was performed with the SeeDB2 method (Ke et al. 2016) with modifications. Tissues were immersed in iohexol containing 0.5% Triton X-100 and incubated at 25 °C overnight. For P7 samples, the SeeDB method (Ke et al. 2013) was used instead. Tissues were incubated in 20% (weight/volume), 40%, 60%, 80%, and 100% fructose for 4–12 h each and then in SeeDB solution [80.2% (weight/weight) fructose] for at least 12 h at 25 °C. For imaging, cleared cortices were mounted in the final clearing solution between two coverslips with silicone rubber spacers.

Confocal Imaging

Cleared, flat-mounted cortices were imaged with a confocal laser scanning microscope (LSM710, Zeiss) equipped with a long-working-distance 20× objective (LD-Plan Neofluar, NA = 0.40, working distance = 8.4 mm, Zeiss) and GaAsP detectors. EGFP was excited with an Argon laser (488 nm), and the laser power was manually adjusted (2–80%) for consistent fluorescent intensities at different depths. Z-stack and tiled images were acquired using a motorized stage and ZEN software (ZEN 2011 SP7 FP1 (black), Zeiss) at a resolution of 512 × 512 pixels for the x- and y-axes (0.84 μm per pixel) and at a 5 μm pitch for the z-axis. The imaging area was determined to include S1 (for P3) and both S1 and M1 (for P5 and P7) from the pial surface to the bottom of the white matter.

Axon Tracing

Three-dimensional reconstruction of confocal images and tracing of axons were performed using Neurolucida® software (version 11, MBF Bioscience). Axons of labeled neurons in the S1 area (mostly in the barrel field) were traced by manually registering the axonal fragment on each focal plane starting from the cell soma to the axonal tips. When ambiguous crossovers with branches derived from other cells were observed, the neurons were excluded from quantifications. At P7, axons of some neurons that extended beyond the imaged area, especially those projecting to M1, were traced up to the edge of the imaged area, and were included in the quantification.

Movies were recorded with the 3D visualization function of Neurolucida and saved in avi format. The avi files were edited (trimming and captioning) and exported as mp4 files with Premiere Pro (version 13.1.2, Adobe).

Branch Length Analysis

Lengths of axonal segments (between two neighboring branching points, between the beginning and the first branching point, and between the terminal and the last branching point) were measured using the "segment analysis" function in Neurolucida Explorer (version 11, MBF Bioscience). The length of each collateral was calculated with Microsoft Excel 2013 by summing the segment length from the branching point on the main shaft to the terminal of the longest of the sub-branches. The branch with the largest measurement value was defined as the longest branch (Max). The average length of all but the longest branch (Average) was calculated for neurons with more than three collateral branches.

Quantification and Statistical Analyses

Double Labeling with Plxnd1 *ISH and Retrograde Tracing*

Three mice were subjected to FG injection at each injection site (ipsilateral M1 and contralateral S1). The numbers of FG-positive neurons and *Plxnd1*/FG-double-positive neurons in the S1 barrel field were counted in layers 2/3 and 5a separately using the "Cell Counter" plug-in for ImageJ (NIH). For the neurons densely stained with ISH, the presence of DAB signals was verified first by shifting the hue of the images (hue, −45; saturation, 55; color balance, 40, 0, −100; and tone balance, Midtones) in Photoshop CS3 (Adobe). The hue-shifted images were then subjected to processing with the "Color Deconvolution" plug-in for ImageJ (Ruifrok and Johnston 2001). Using the H (hematoxylin) -DAB vector in the plug-in, ISH + IHC images were deconvoluted into three channels (H, DAB, and green channels), and signals that appeared in the DAB-channel were treated as positive cells. For the neurons that were densely stained with DAB, the presence of ISH signals was verified by comparing ISH + IHC images and the corresponding ISH-only images. The data are presented as the mean ± SEM of three mice for each injection site/layer combination.

Double Labeling with Plxnd1 *ISH and Anti-GFP Immunohistochemistry*

A mouse at P29 and three mice at P10 were subjected to analysis. The numbers of GFP-positive neurons and GFP/*Plxnd1*-double-positive neurons were counted using the "Cell Counter" plug-in for ImageJ. The data are presented as the mean ± SEM of three mice at P10. Inclusion of P29 data did not greatly change the mean value (not shown).

Branch Length Analysis

Three pups at each developmental stage (P3, P5, and P7) were subjected to imaging and analysis. Analysis was restricted to the intensely labeled neurons with more than two collaterals, one of which was a projection in the direction of M1 and was longer than the others. The branch length of the collaterals was measured for n = 7, 10, and 18 neurons at P3 (N = 2 mice), P5 (N = 3 mice), and P7 (N = 3 mice), respectively. Nonparametric statistical analyses were performed using JMP® Pro (version 15; SAS

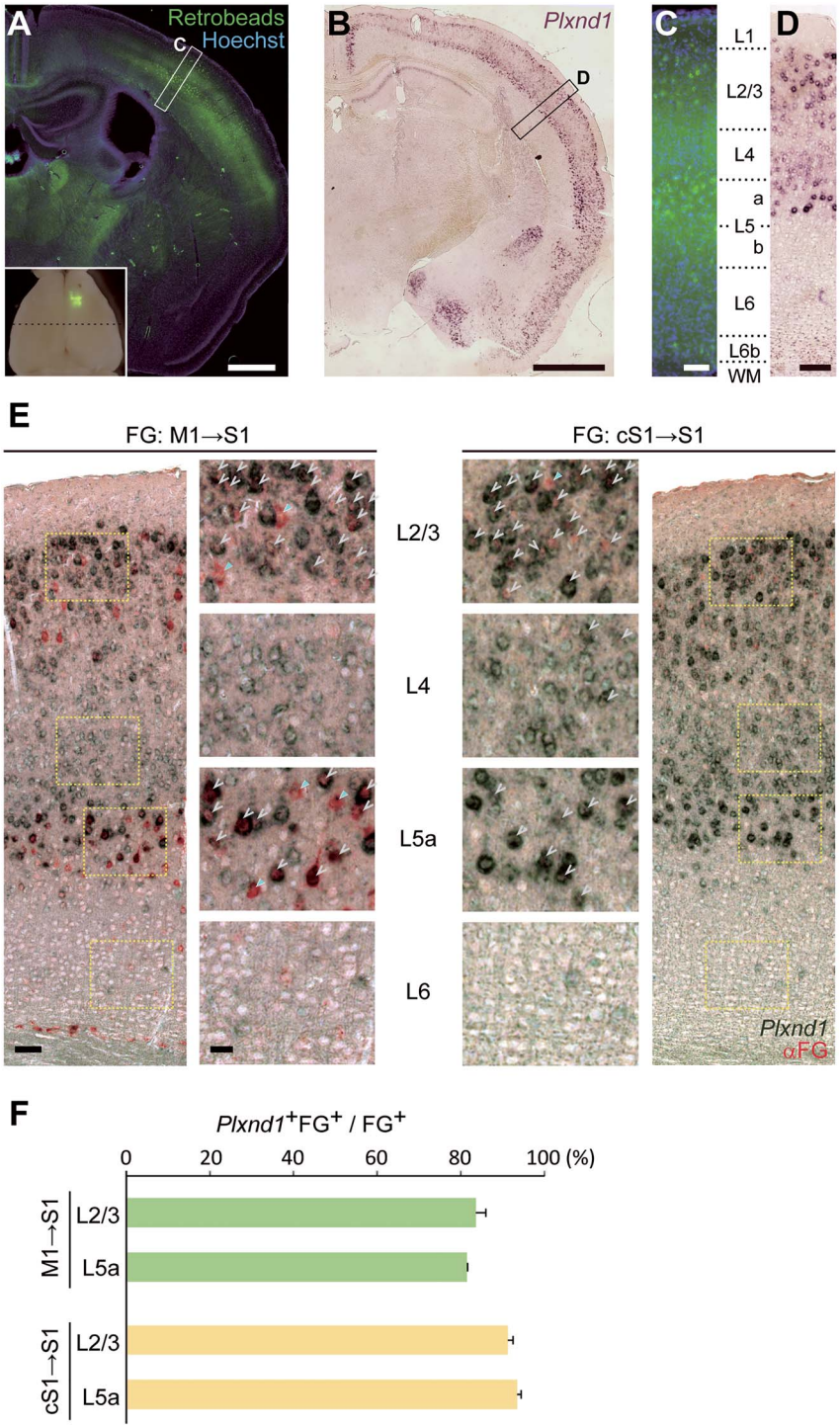

Figure 1. The *Plxnd1* gene is expressed in M1-projecting and cS1-projecting neurons in layers 2/3 and 5a in S1. (A) Coronal section at the level of S1 of the mouse brain 3 days after injection with Green Retrobeads into M1 at P21. Retrogradely labeled cell bodies were detected in S1. The boxed area in S1 is shown at higher magnification as (C). Scale bar, 1 mm. Inset: Injection site from the dorsal view of the whole mount brain. The dashed line indicates the level of the coronal section. Section counterstained with Hoechst (blue). **(B)** Expression of the *Plxnd1* gene using ISH with coronal sections at P29. Two major expression bands were detected in layers 2/3 and 5. The boxed area in S1 is shown at a higher magnification in (D). Scale bar, 1 mm. **(C, D)** Comparison of labeling patterns in S1 between retrograde labeling from M1 to S1 (C) and *Plxnd1* expression (D). Neurons in the same layers (2/3 and 5a) were labeled in both experiments. Scale bars, 100 µm. **(E)** Coronal sections at P26 injected with Fluoro-Gold (FG) at P21 were subjected to ISH for *Plxnd1* (dark green). FG was detected with anti-FG antibody (α-FG, orange). Note that hue of the images was uniformly shifted from that of the original images (See Supplementary Figure S1). Left: FG was injected into M1 (M1 → S1). Right: FG was injected into contralateral S1 (cS1 → S1). Higher magnification images of each layer (yellow dashed boxes) are shown in the middle panels. The arrowheads in gray and cyan indicate double-positive and FG-positive cells. Scale bars, 100 µm and 20 µm for low and high magnifications, respectively. **(F)** Quantification of double labeling experiments. Data are represented as the mean ± SEM. N = 3 mice for each FG-injection site.

Institute Inc., Cary, NC, USA). For comparison of the difference in length between Max and Average, the two-tailed Wilcoxon rank sum test was used. For comparison of Max, Average, or Ratio (Max/Average) between stages (P3 versus P5, P3 versus P7, and P5 versus P7), the two-tailed Steel-Dwass multiple comparison test was used. Data are presented as box-and-whisker plots with individual data points. Center line, median; box edges, upper and lower quartiles; whiskers, maximum and minimum data points within the 1.5× interquartile range.

Results

The Majority of S1 Neurons with Association Projections to M1 Express *Plxnd1*

Retrograde tracing showed that neurons with association projections from the barrel field in S1 to M1 were localized to three layers: layers 2/3, 5, and 6b (Fig. 1A), which is consistent with preceding studies (Mitchell and Macklis 2005; Watakabe et al. 2012). The *Plxnd1* gene is expressed in layers 2/3 to 5a of the adult mouse S1 barrel field (Watakabe et al. 2006). Our ISH analysis confirmed the strong expression of *Plxnd1* in layers 2/3 and 5a with weaker expression in layer 4 at P29 (Fig. 1B). We assumed that the strong expression in layers 2/3 and 5a might correspond to the expression in the retrogradely labeled cells (Figs 1C and 1D). We performed double labeling experiments with retrograde tracing using FG and ISH for *Plxnd1* to verify whether M1-projecting neurons in S1 expressed *Plxnd1*. We detected double-positive cells in layers 2/3 and 5a, which confirmed the expression of *Plxnd1* in M1-projecting neurons in S1 (Fig. 1E and Supplementary Figure S1). Over 80% of retrogradely labeled cells in both layers 2/3 and 5a were *Plxnd1*-positive (Fig. 1F). In contrast, very few double-positive neurons were detected in other layers, not even in layer 4 where *Plxnd1* was expressed in many cells at lower levels (Fig. 1E).

In a parallel experiment where the tracer was injected into contralateral S1, we found that over 90% of callosally projecting neurons in layers 2/3 and 5a expressed *Plxnd1* (Figs. 1E and 1F, and Supplementary Figure S1). In layer 4 with a low level of *Plxnd1* expression, only a very small number of double positive cells were detected (Fig. 1E). These results corroborate the study that established *Plxnd1* as a marker for callosally projecting neurons in layers 2/3 and 5a (Molyneaux et al. 2009). Taken together, these data suggest that these S1 neurons project both ipsilaterally and contralaterally.

Developing a Sparse Labeling Method for Cortical Neurons Using the *Plxnd1* Promoter

Based on the high percentage of *Plxnd1*-expressing neurons among M1-projecting neurons in layers 2/3 of S1, we constructed a pPlxnd1-Cre plasmid by placing the DNA recombinase gene *Cre* downstream of the promoter of *Plxnd1* to visualize the association projection of *Plxnd1*-expressing neurons. The promoter region in our construct spanned 16.4 kb upstream of the start codon, containing five regions homologous to the human *Plxnd1* gene (Supplementary Figure S2). The fidelity of the promoter was tested by performing IUE with pPlxnd1-Cre and the Cre-dependent reporter plasmid pCALNL-GFP, followed by double staining with ISH for *Plxnd1* and IHC against GFP. Nearly all GFP-expressing cells were *Plxnd1*-positive (Fig. 2). In addition, GFP expression driven by the *Plxnd1* promoter was found to be restricted in the cells expressing SATB2, an established callosal neuron marker (Fig. 3: Alcamo et al. 2008; Britanova et al. 2008).

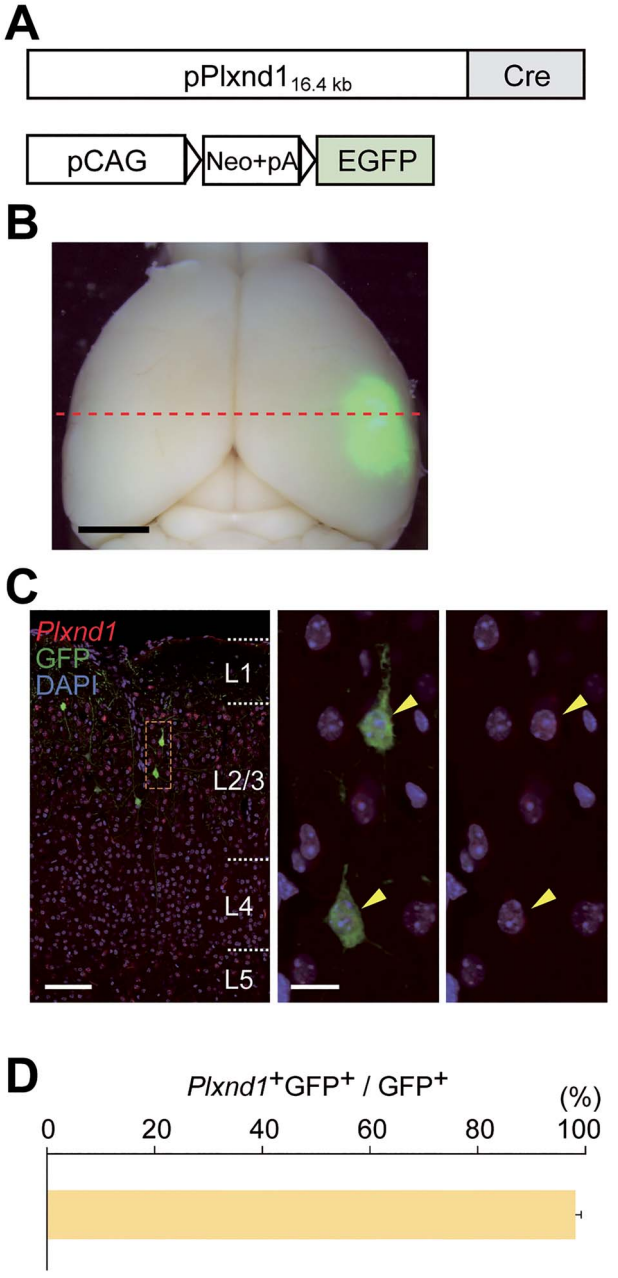

Figure 2. The promoter of *Plxnd1* recapitulates the endogenous *Plxnd1* expression pattern. (A) Schematic drawing of the plasmid vectors, pPlxnd1-Cre and pCALNL-GFP, used for IUE at E15.5. Triangles, loxP sequence. **(B)** Dorsal view of the electroporated brain dissected at P29. Bright field image was overlaid on the green fluorescent image. The red dashed line indicates the level of coronal sections used for double staining shown in (C). Scale bar, 2 mm. **(C)** ISH for *Plxnd1* and immunohistochemistry against GFP. The area boxed with the orange dashed line is shown at a higher magnification in the middle and right panels. Yellow arrowheads, double-positive neurons. Scale bars, 100 µm for the left panel, 20 µm for the middle and right panels. **(D)** Quantification of double labeling experiment. The ratio of double-positive neurons over GFP-positive neurons is represented as the mean ± SEM. N = 3 mice at P10.

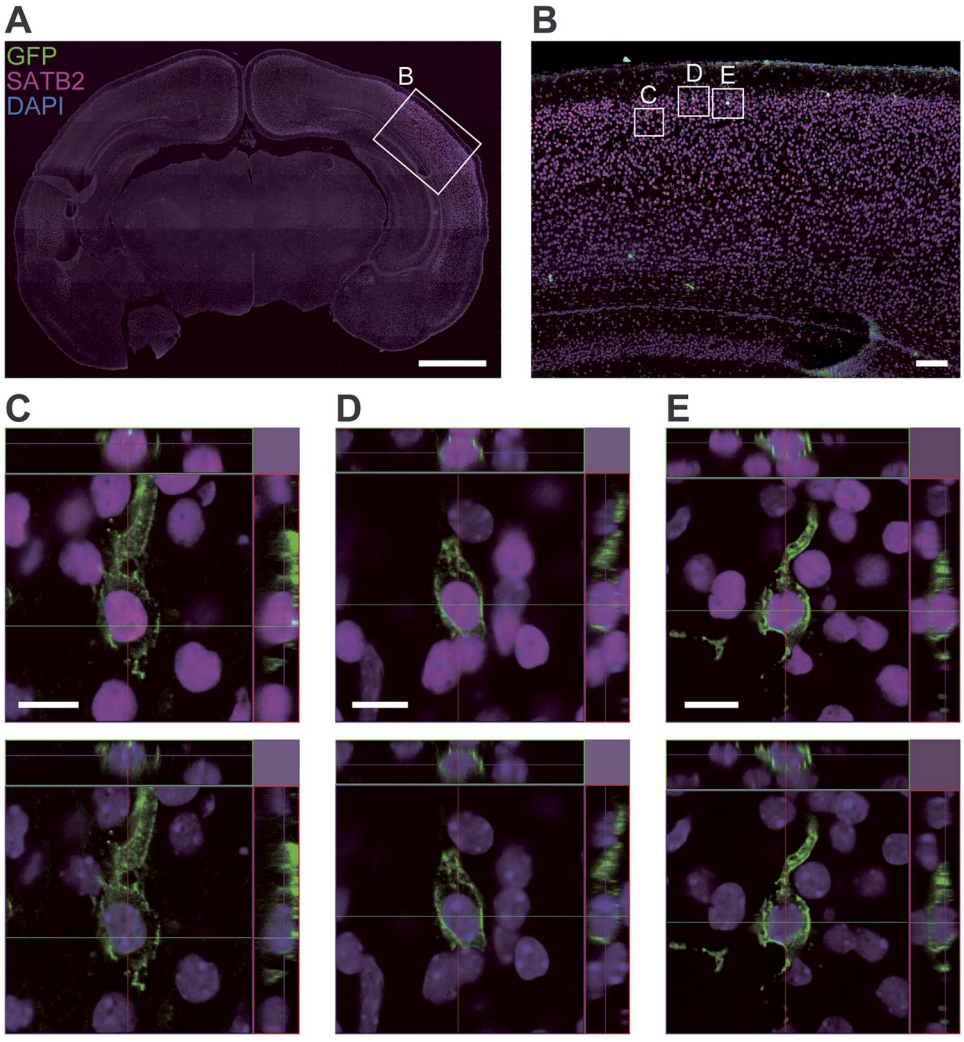

Figure 3. GFP expression driven by the *Plxnd1* promoter detected in SATB2-expressing neurons. (A) Double immunohistochemistry for anti-GFP (green) and anti-SATB2 (magenta) with a coronal section of P5 brain that was electroporated with pPlxnd1-Cre and pCA-mTmG at E15.5. The section is counterstained with DAPI (blue). **(B)** A higher magnification view of the S1 area (boxed in A). **(C–E)** Higher magnification views of GFP-positive cells in layer 2/3 (boxed in B). A single z-plane with vertical and horizontal lines indicating the cutting planes for the orthogonal views shown on right and top of each image. Top panels, all three channels. Bottom panels, same images without magenta channel to show nuclear staining with DAPI. Scale bars, 1 mm (A), 100 µm (B), and 10 µm (C–E).

We used this driver plasmid together with the Cre-dependent reporter pCA-mTmG, in which the expressed fluorescent reporter was switched from membrane-bound tdTomato to membrane-bound EGFP upon recombination, to visualize the projection of the labeled neurons to M1. However, when layer 2/3 neurons were labeled using these plasmids with IUE at E15.5, GFP expression in the axons was too faint to be followed up to M1 for many *Plxnd1*-expressing neurons despite clear labeling of cell bodies and dendrites in S1 during the early postnatal stages. As the expression of *Plxnd1* in layer 2/3 was detectable but rather weak at P1, P3, and P5 (Fig. 4), it was likely that insufficient expression of Cre driven by the *Plxnd1* promoter resulted in incomplete reporter switching in many cells. On the other hand, the importance of sparse labeling in the reconstruction of axon collaterals using light microscopy has been emphasized (Economo et al. 2016). We therefore constructed a new Cre-dependent Cre expression vector (pCAGGS-DIO-iCre) that improved the recombination efficiency in many cells and led to higher expression of EGFP while maintaining labeling sparsity (Fig. 5).

A Single *Plxnd1*-Expressing Layer 2/3 Neuron Projects to M1 and the Contralateral Hemisphere

IUE using pPlxnd1-Cre, pCA-mTmG, and pCAGGS-DIO-iCre enabled successful visualization of entire axons of many *Plxnd1*-expressing layer 2/3 neurons. We analyzed brain samples at different postnatal days by confocal imaging of flat-mounted cortices that were optically cleared using the SeeDB (Ke et al. 2013) or SeeDB2 (Ke et al. 2016) method (Fig. 6, Supplementary Figures S3, S4, and S5). When we observed them at P7, we detected hundreds of GFP-labeled layer 2/3 neurons, although the signal intensity varied. Among the neurons with sufficient labeling to trace to the axon terminals, we found that 18 neurons (in three mice) had a long association projection to M1 and a callosal projection (Supplementary Tables S1, S2),

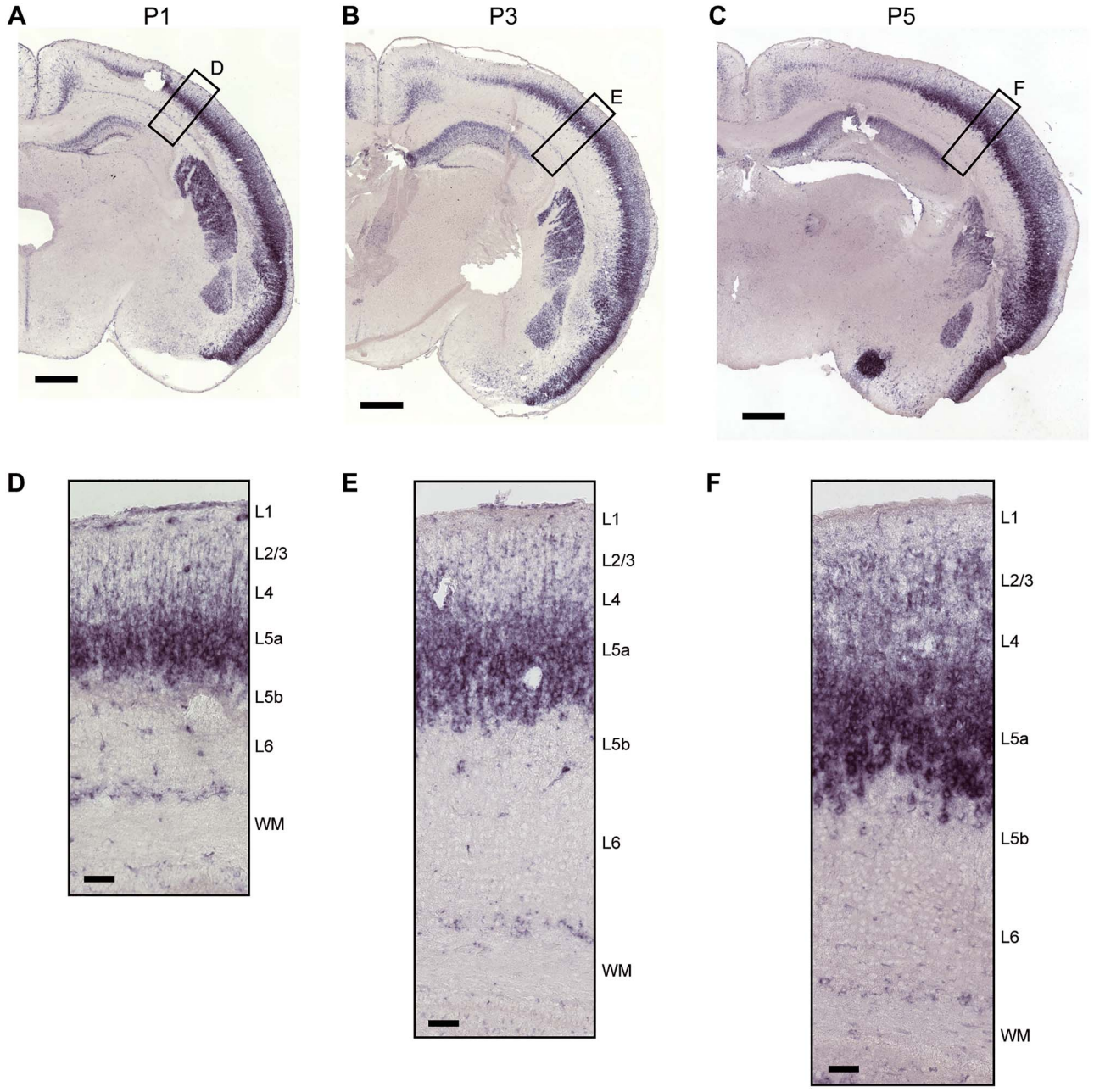

Figure 4. *Plxnd1* expression in S1 at early postnatal stages. (A–C) *Plxnd1* expression was examined by ISH with coronal sections at P1 (A), P3 (B), and P5 (C). Scale bars, 500 µm. **(D–F)** Higher magnification images of boxed areas in (A–C). Layers are indicated on the right. Scale bars, 50 µm.

conforming to previously described dual-projection neurons (Mitchell and Macklis 2005; Yamashita et al. 2013). Generally, the main axon of each neuron extended vertically down to the white matter, where it made a right turn toward the midline. Within the gray matter before entering the white matter, it branched primarily at the level of layer 5. Less branching was observed in other layers. The long association projection of each neuron was by far the longest of those branched at the level of layer 5. (Fig. 6 Supplementary Figure S5, and Supplementary Movies S1, S2, S3, and S4). The long association projections to M1 showed a characteristic trajectory: first heading downwards obliquely to layer 6 and turning up toward the pia before reaching the white matter (Fig. 6, xz-projection; Supplementary Movies S3 and S4). As a population, they did not form a tight bundle but coursed to M1 through various routes that were distinct in their levels and lateral positions.

The Projection to M1 of a *Plxnd1*-Expressing Layer 2/3 Neuron Develops as the Longest among the Axon Collaterals in each Neuron

We next analyzed the developmental changes in the association projection from *Plxnd1*-expressing neurons to M1 by

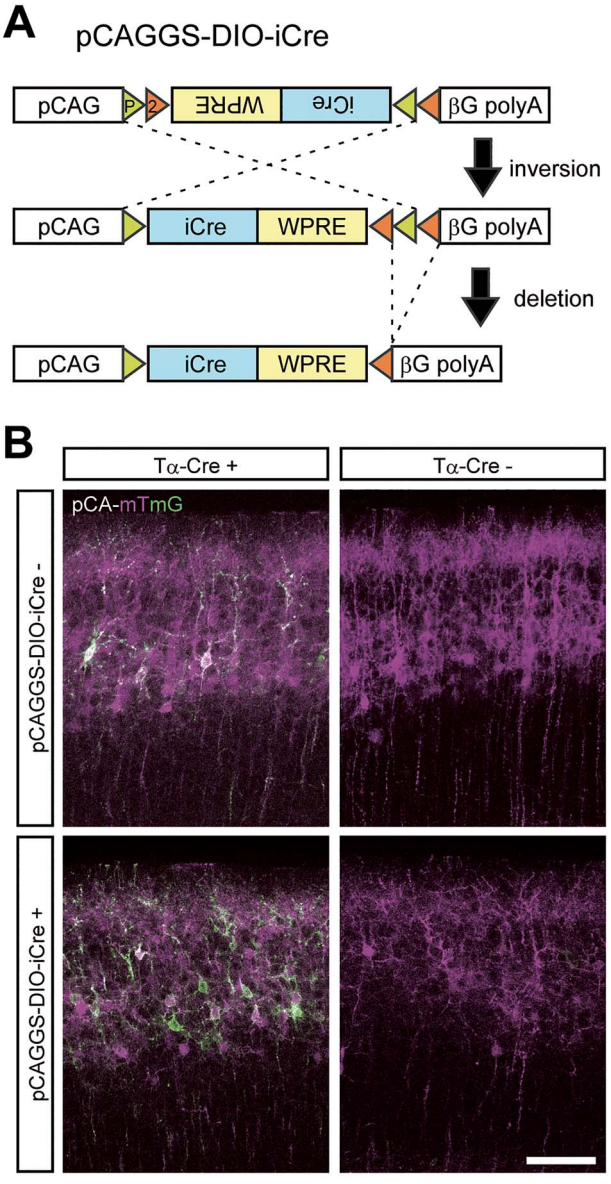

Figure 5. A novel plasmid construct for improved sparse labeling. (A) Schematic drawing of the novel vector, pCAGGS-DIO-iCre, and its Cre-mediated induction of iCre expression. P, loxP; 2, lox2272; WPRE, woodchuck hepatitis virus post-transcriptional regulatory element. βG polyA, rabbit β-globin 3′UTR sequence. **(B)** The improvement of sparse labeling with pCAGGS-DIO-iCre was tested by introducing Tα-Cre, pCA-mTmG, and pCAGGS-DIO-iCre into L2/3 neurons with IUE at E15.5. Coronal sections were examined at P5. Cre-mediated recombination of pCA-mTmG changed the expression of the reporter from tdTomato (magenta) to EGFP (green). More green cells were detected in the presence of pCAGGS-DIO-iCre than in its absence. White cells were positive for both tdTomato and EGFP, suggesting that Cre expression was not sufficient in these cells to recombine all the pCA-mTmG plasmid molecules taken up. Scale bar, 100 µm.

comparing among the cortices sampled at P3, P5, and P7 (Fig. 7, Supplementary Figures S3, S4, and S5). While the projection to the contralateral hemisphere crossed the midline at birth (data not shown), branching in the cortex first emerged at P3 in the large majority of the labeled neurons (Fig. 7A, 77.8% of 36 neurons, N = 3 mice. In a separate set of experiments, the percentage of labeled neurons with branches at the level of layer 5 was only 17.6% of 152 neurons, N = 2 mice, at P2). This result indicated that cortical branching emerged as axon collaterals (Hand et al. 2015; Srivatsa et al. 2015). Even at P3, the collateral branches of a single neuron had different lengths, and the longest branch grew even longer over the course of development compared to the remaining shorter branches. We selected all the neurons with intense labeling and with the longest collaterals in the direction of M1 at P3, P5, and P7 to measure the lengths of all collaterals in each neuron. Because M1-projecting axons of some neurons at P7 extended beyond the imaged area, our measurement might have underestimated their length. Even so, comparison between the length of the longest collateral (Max) and the average length of the other collaterals (Average) in each neuron clearly demonstrated that the difference increased as development proceeded (Fig. 7B, Supplementary Table S3). The increase in the Max/Average ratio further indicated that the observed difference became larger in later stages (Fig. 7C, Supplementary Table S3). Although the difference was not significant at P3, the Max/Average ratio was approximately 2 (median = 2.04, mean = 2.12; Supplementary Table S3). Together, these results raised the possibility that a single collateral from an individual *Plxnd1*-expressing layer 2/3 neuron was selected at a very early stage of collateral development to target a distant area.

Discussion

Using single-neuron tracing, we demonstrated that most long association projections from layer 2/3 neurons in S1 to M1 arose as interstitial collaterals that extended postnatally from existing callosal axons. This conclusion is consistent with the prenatal establishment of callosal projections followed by projections to frontal areas (Mitchell and Macklis 2005). We further demonstrated that these neurons developed as dual-projection neurons, in which both callosal and association axons extended simultaneously from P3 to P7.

We developed an advanced tracing method to overcome the limitations of existing tracing approaches. We were not able to use classical retrograde tracer injection experiments or a more up-to-date RNAseq-based mapping of neuronal projections (Kebschull et al. 2016), since both approaches require axons to have reached their target. Since collateral projection occurs during early postnatal development, the popular approach for circuit analysis using AAVs is limited by the waiting period for protein expression after virus injection. Our method overcomes these limitations and provides a simple and efficient way to analyze developing axons of cortical neurons, which includes growth cone trajectory and temporal changes in axon branching patterns. Our new Cre-amplifying vector, pCAGGS-DIO-iCre, is a useful tool to improve the efficiency of any sparse labeling experiment based on a Cre/loxP system.

Preceding studies suggested that dual-projection of cortical pyramidal neurons is a transient event during development: neurons lose one of the two long branches during their postnatal circuit maturation processes (Ivy et al. 1979; O'Leary et al. 1981; Ivy and Killackey 1982). However, more evidence has emerged to show that dual-projection neurons exist in the adult cortex (Schwartz and Goldman-Rakic 1982; Mitchell and Macklis 2005; Yamashita et al. 2013, 2018; Watakabe et al. 2014), implying a more permanent feature. Our results suggest that most, if not all, association projections arise as collateral branches emerging from callosal axons of dual-projection neurons. A recent study reported a significant reduction in callosal projections of layer

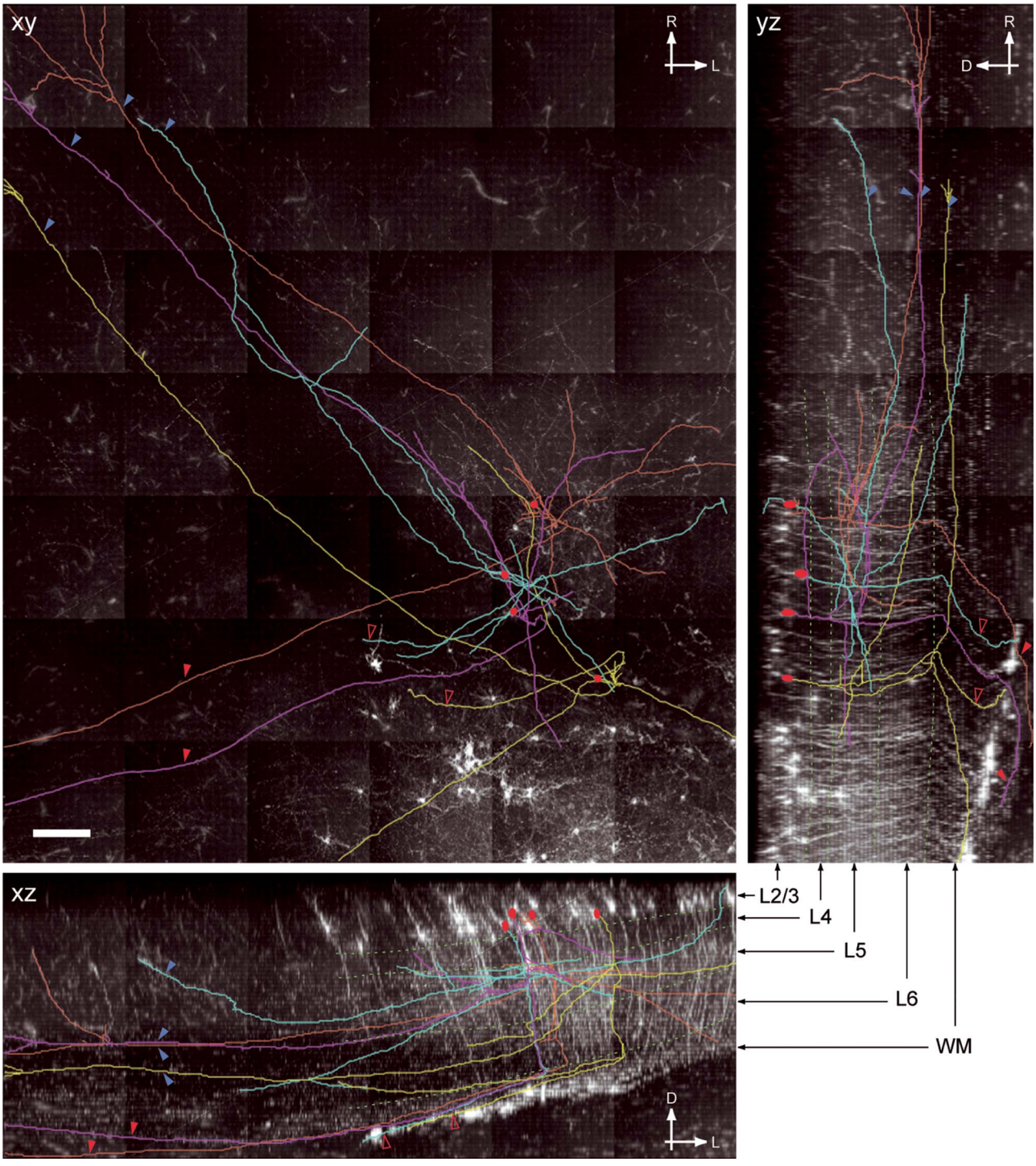

Figure 6. Individual *Plxnd1*-expressing neurons in layer 2/3 have axons projecting both to ipsilateral M1 and to contralateral S1. *Plxnd1*-expressing neurons in layer 2/3 in S1 were labeled by introducing pPlxnd1-Cre, pCA-mTmG, and pCAGGS-DIO-iCre with IUE at E15.5. The cortices were removed at P7, then flattened, optically cleared, and imaged with confocal microscopy. The maximum-intensity projections of the EGFP signals (white) onto the xy-, xz-, and yz-planes are presented. Neurolucida traces of the axons of four example neurons with projections to M1 are shown in different colors. Red ovals, cell bodies; red filled arrowheads, callosally projecting axons; red open arrowheads, axons projecting along the callosally projecting axons but terminating in the white matter; blue arrowheads, axons projecting in the direction of M1; Green dotted curves, layer borders; WM, white matter; R, rostral; L, lateral; and D, dorsal. Please note that the M1-projecting axon of the yellow neuron looks extending through the white matter in the yz-projection due to the tilt of the sample against the xy-plane as seen in the xz-projection. For better visualization, see Supplementary Movies S3 and S4. Scale bar, 200 μm.

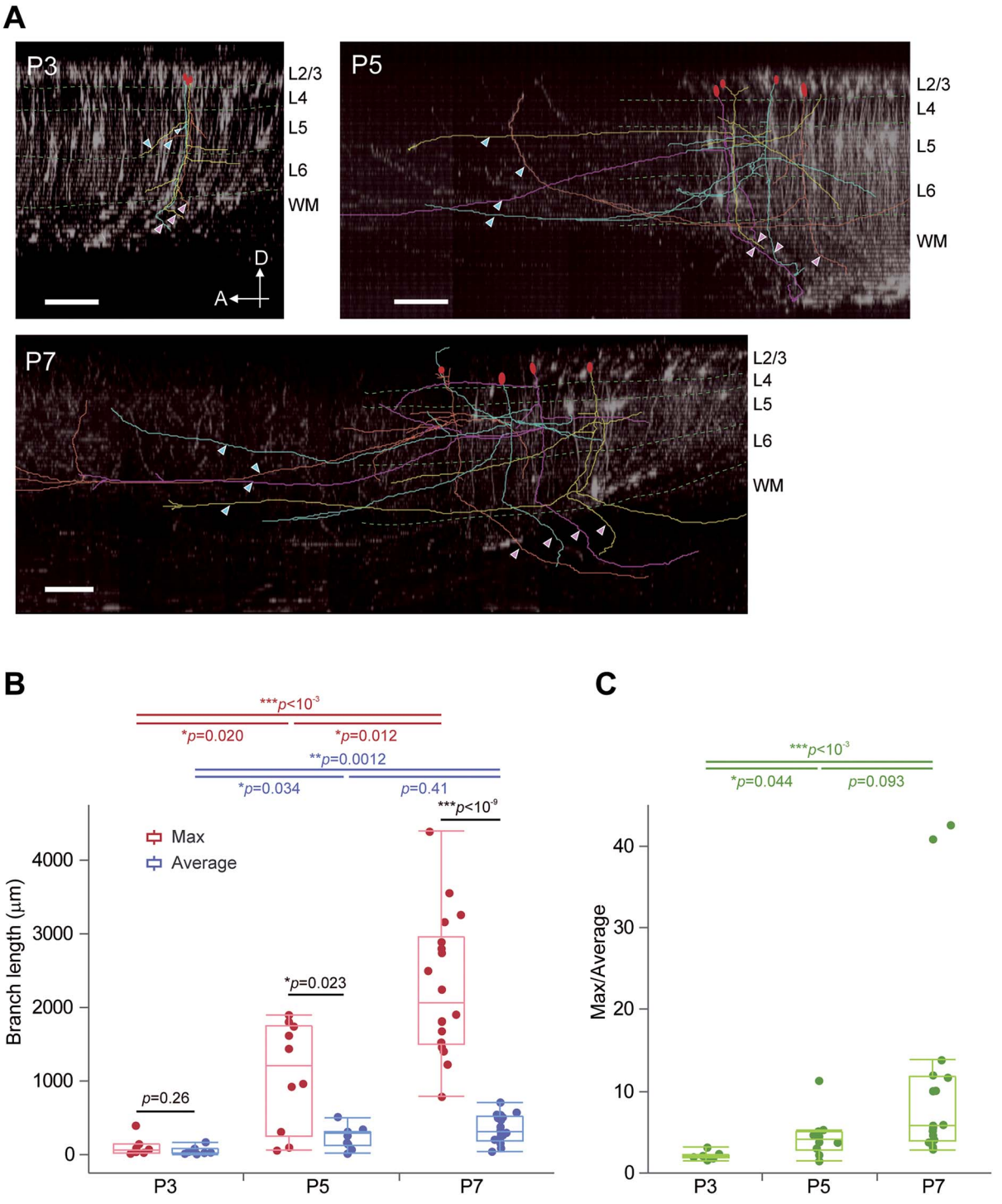

Figure 7. Interareal connections to M1 develop as interstitial axon collaterals. (A) Traced axons of *Plxnd1*-expressing L2/3 neurons with projections in the direction of M1 in the brain samples that were electroporated at E15.5 and analyzed at P3, P5, and P7. Only the xz-projections are shown. Red ovals, cell bodies; red arrowheads, callosally projecting axons; blue arrowheads, axons projecting in the direction of M1; Green dotted curves, layer borders. Scale bars, 200 μm. **(B, C)** Quantitative analysis of branch length. Difference between the length of the farthest reaching branch (Max) and the average length of the remaining branches (Average) of each neuron became greater in the later stages (B, two-tailed Wilcoxon rank sum test for comparison between Max and Average; two-tailed Steel-Dwass multiple comparison test for comparison between stages). The ratio of Max/Average also increased in later stages (C, two-tailed Steel-Dwass multiple comparison test). Data are presented as box-and-whisker plots with individual data points. Center line, median; box edges, upper and lower quartiles; whiskers, 1.5× interquartile range. n = 7, 10, and 18 neurons for P3, P5, and P7 (pooled from 2, 3, and 3 mice at each stage).

2/3 neurons in S1 during postnatal development (De León Reyes et al. 2019). Similar reductions are also reported in primates (Innocenti et al. 1977; LaMantia and Rakic 1990). Since our study focused on the initial phase of circuit formation particularly the process until the axons reach their target, it is still possible for future work to clarify whether some of these dual-projection neurons become bona fide association neurons after losing a callosal projection.

Recent studies have shown that both rodents and ferrets share similar fiber layer structures in the cerebral cortex with primates: the outer fiber layer of intracortical projections and the inner fiber layer of intercortical and subcortical projections (Kawasaki et al. 2013; Saito et al. 2019). Since our results demonstrate that a single neuron possesses both intracortical (association) and intercortical (callosal) projections, we propose that association projections formed as interstitial collaterals from dual-projection neurons constitute a conserved mechanism among the mammalian species. Interestingly, in a retrograde tracing experiment in the cat visual cortex, association projections (from area 17 to area 18) of some upper layer neurons were eliminated, leaving labeled neurons in a patchy distribution (Price and Blakemore 1985). An intriguing future direction will be to examine whether this is a shared phenomenon among sensory cortices and among species. The patches in the visual cortex might correspond to barrels (or regions directly above them) in S1. On the other hand, anterograde labeling studies of axons in the developing cat visual cortex suggest that random, exuberant projection followed by specific elimination underlies the formation of corticocortical connections (Callaway and Katz 1990). Judging from the collateral lengths analyzed in this study and the size of area 17 in carnivores, this is most likely a local event within area 17. As we did not find more than a few, if not a single, long collaterals extending beyond S1 in random directions, it is conceivable that distinct mechanisms underlie the formation of long-range and local association connections.

Topographic projections from S1 to M1 are known (Mao et al. 2011), while the projection from the barrel cortex to the contralateral hemisphere is more abundant in areas lateral to the barrel cortex than in the barrel cortex itself (Fenlon et al. 2017). Sister neurons produced from the same radial glial cell in S1 are more likely to connect with another set of sister neurons in M1, while connecting partners in cS1 are not clonally related (Ren et al. 2019). These findings suggest that different guidance and elimination mechanisms operate between M1-projecting collaterals and cS1-projecting callosal axons of a given dual-projection neuron. The trajectory of the association collateral to M1 of *Plxnd1*-expressing layer 2/3 neurons showed little branching before reaching its target. This result favors a directed guidance mechanism operating in specific branches over a two-step mechanism with initial random projections followed by elimination of unnecessary branches. The routes of association collaterals to M1 varied from cell to cell. Thus, we conclude that fasciculation of axon branches is less likely to play an important role in the guidance of collaterals.

Because these branches did not enter the white matter as observed for long-range interareal connections in primates (Rockland 2013), each branch must navigate to its distant target through the neuron-rich gray matter. As the projection from S1 to M1 also comprises neurons in layers 5a and 6b (Fig. 1A), it is possible that collaterals of layer 2/3 neurons follow axonal scaffolds presented by deep-layer neurons.

Another possible mechanism of collateral guidance may utilize reciprocal navigation between M1-projecting axons of S1 neurons and S1-projecting axons of M1 neurons, as described by the well-known hand-shake model between the cortex and the thalamus (Deck et al. 2013). Interestingly, S1 also has reciprocal connections with S2, but the feedback projections from S2 originate from layer 4 instead (Minamisawa et al. 2018), hence creating further diversity in collateral guidance mechanisms. Another intriguing evidence is that *Sema3e*, a gene that encodes a specific ligand for Plxnd1, is localized in layer 5b and 6 neurons in a complementary manner to *Plxnd1* expression (Watakabe et al. 2006). A preceding study that analyzed axon projections of cortical neurons in *Plxnd1*- or *Sema3e*-knockout mice revealed that callosal neurons in M1 with heterotopic projections to the striatum showed an upward shift in laminar distribution (Velona et al. 2019). Our preliminary attempts to disrupt Plxnd1/Sema3E signaling by shRNA-mediated gene knockdown and CRISPR/Cas9-mediated gene knockout of *Plxnd1* in layer 2/3 neurons of S1 did not show obvious differences in collateral formation or projection to M1 (data not shown). Future studies should address the molecular mechanisms that underlie the guidance of association collaterals.

Our results suggest that at an early stage of extension, a single collateral is selected among "sibling" collaterals for targeting a distant area. As a population, axons of layer 2/3 neurons in S1 simultaneously innervate multiple target areas M1, S2, and cS1, each at a different distance from where the soma resides (Hand et al. 2015). Thus, our findings suggest that both delayed collateral budding and the distinct extension speeds of collateral branches, which vary according to the distance to the respective target area, may contribute to simultaneous circuit formation by a single layer 2/3 neuron at multiple targets.

In conclusion, we uncovered the developmental processes of dual-projection neurons and revealed that their axon collaterals comprise association projections. Since association projections are most elaborate in primates such as humans, our findings substantially contribute to a unified foundation to understand the development and evolution of cortical networks that underlie human cognitive functions.

Supplementary Material

Supplementary material can be found at *Cerebral Cortex* online.

Funding

This work was supported by grants from Takeda Science Foundation; NOVARTIS Foundation (Japan) for the Promotion of Science; Naito Foundation; and Japanese Society for Promoting Science (JPSP KAKENHI grant numbers JP23800027, JP24700352, JP25123704, JP26830027, JP17K07076, and JP21K06409 to Y.O. and JP15K15015, JP25293043, JP17H04014, and JP20H03414 to M.S.).

Notes

We thank M.-T. Ke and T. Imai for advice on optical clearing and T. Miyata, L Luo, C. Cepko, and J. Kim for providing plasmid constructs. We are grateful to H. Yoshikawa, S. Kanae, I. Kumano, H. Miyagoshi, C.-C. Wang, A. Emi, T. Nishiguchi, and M. Matsuda for technical assistance; S. Yasumura, K. Kuroda, M.-J. Xie, Y. Mori, and H. Yagi for helpful discussion; and T. Taniguchi, M. Yamaguchi, Y. Shibuya, A. Yoshinori, and K. Danke for secretarial assistance. We thank Life Science Editors and Nature Research Editing Service for editing assistance. The imaging experiments

were supported by the Center for Medical Research and Education, Graduate School of Medicine, Osaka University. Animal experiments were supported by the Life Science Research Laboratory, University of Fukui, and The Institute of Experimental Animal Science, Faculty of Medicine, Osaka University. *Conflict of Interest*: The authors declare no competing financial interests.

References

Alcamo EA, Chirivella L, Dautzenberg M, Dobreva G, Fariñas I, Grosschedl R, McConnell SK. 2008. Satb2 regulates callosal projection neuron identity in the developing cerebral cortex. *Neuron*. 57:364–377.

Britanova O, de Juan Romero C, Cheung A, Kwan KY, Schwark M, Gyorgy A, Vogel T, Akopov S, Mitkovski M, Agoston D, Šestan N, Molnár Z, Tarabykin V. 2008. Satb2 is a postmitotic determinant for upper-layer neuron specification in the neocortex. *Neuron* 57:378–392.

Callaway EM, Katz LC. 1990. Emergence and refinement of clustered horizontal connections in cat striate cortex. *J Neurosci*. 10:1134–1153.

Chiang HL, Chen YJ, Lin HY, Tseng WYI, Gau SSF. 2017. Disorder-specific alteration in white matter structural property in adults with autism spectrum disorder relative to adults with ADHD and adult controls. *Hum Brain Mapp*. 38:384–395.

Coogan TA, Burkhalter A. 1993. Hierarchical organization of areas in rat visual cortex. *J Neurosci*. 13:3749–3772.

De León Reyes NS, Mederos S, Varela I, Weiss LA, Perea G, Galazo MJ, Nieto M. 2019. Transient callosal projections of L4 neurons are eliminated for the acquisition of local connectivity. *Nat Commun*. 10:4549.

Deck M, Lokmane L, Chauvet S, Mailhes C, Keita M, Niquille M, Yoshida M, Yoshida Y, Lebrand C, Mann F, et al. 2013. Pathfinding of corticothalamic axons relies on a rendezvous with thalamic projections. *Neuron*. 77:472–484.

Druckmann S, Feng L, Lee B, Yook C, Zhao T, Magee JC, Kim J. 2014. Structured synaptic connectivity between hippocampal regions. *Neuron*. 81:629–640.

Economo MN, Clack NG, Lavis LD, Gerfen CR, Svoboda K, Myers EW, Chandrashekar J. 2016. A platform for brain-wide imaging and reconstruction of individual neurons. *eLife*. 5:e10566.

Felleman DJ, Van Essen DC. 1991. Distributed hierarchical processing in the primate cerebral cortex. *Cereb Cortex*. 1:1–47.

Fenlon LR, Suárez R, Richards LJ. 2017. The anatomy, organisation and development of contralateral callosal projections of the mouse somatosensory cortex. *Brain Neurosci Adv*. 1:1–9.

Fitzgerald J, Leemans A, Kehoe E, O'Hanlon E, Gallagher L, McGrath J. 2018. Abnormal fronto-parietal white matter organisation in the superior longitudinal fasciculus branches in autism spectrum disorders. *Eur J Neurosci*. 47:652–661.

Fletcher LN, Williams SR. 2019. Neocortical topology governs the dendritic integrative capacity of layer 5 pyramidal neurons. *Neuron*. 101:76–90.e4.

Franklin KB, Paxinos G. 2008. *The Mouse Brain in Stereotaxic Coordinates*. Compact 3rd ed. Amsterdam (Netherlands): Elsevier Academic Press.

Goldman PS, Nauta WJH. 1977. Columnar distribution of cortico-cortical fibers in the frontal association, limbic, and motor cortex of the developing rhesus monkey. *Brain Res*. 122:393–413.

Greig LC, Woodworth MB, Galazo MJ, Padmanabhan H, Macklis JD. 2013. Molecular logic of neocortical projection neuron specification, development and diversity. *Nat Rev Neurosci*. 14:755–769.

Han Y, Kebschull JM, Campbell RAA, Cowan D, Imhof F, Zador AM, Mrsic-Flogel TD. 2018. The logic of single-cell projections from visual cortex. *Nature*. 556:51–56.

Hand RA, Khalid S, Tam E, Kolodkin AL. 2015. Axon dynamics during neocortical laminar innervation. *Cell Rep*. 12:172–182.

Hutsler JJ, Lee DG, Porter KK. 2005. Comparative analysis of cortical layering and supragranular layer enlargement in rodent carnivore and primate species. *Brain Res*. 1052:71–81.

Iguchi T, Yagi H, Wang C-C, Sato M. 2012. A tightly controlled conditional knockdown system using the *Tol2* transposon-mediated technique. *PLoS ONE*. 7:e33380.

Innocenti GM, Fiore L, Caminiti R. 1977. Exuberant projection into the corpus callosum from the visual cortex of newborn cats. *Neurosci Lett*. 4:237–242.

Isseroff A, Schwartz ML, Dekker JJ, Goldman-Rakic PS. 1984. Columnar organization of callosal and associational projections from rat frontal cortex. *Brain Res*. 293:213–223.

Ivy GO, Akers RM, Killackey HP. 1979. Differential distribution of callosal projection neurons in the neonatal and adult rat. *Brain Res*. 173:532–537.

Ivy GO, Killackey HP. 1982. Ontogenetic changes in the projections of neocortical neurons. *J Neurosci*. 2:735–743.

Jones EG, Wise SP. 1977. Size, laminar and columnar distribution of efferent cells in the sensory-motor cortex of monkeys. *J Comp Neurol*. 175:391–437.

Jou RJ, Mateljevic N, Kaiser MD, Sugrue DR, Volkmar FR, Pelphrey KA. 2011. Structural neural phenotype of autism: preliminary evidence from a diffusion tensor imaging study using tract-based spatial statistics. *Am J Neuroradiol*. 32: 1607–1613.

Katz J, d'Albis MA, Boisgontier J, Poupon C, Mangin JF, Guevara P, Duclap D, Hamdani N, Petit J, Monnet D, et al. 2016. Similar white matter but opposite grey matter changes in schizophrenia and high-functioning autism. *Acta Psychiatr Scand*. 134:31–39.

Kawasaki H, Toda T, Tanno K. 2013. *In vivo* genetic manipulation of cortical progenitors in gyrencephalic carnivores using *in utero* electroporation. *Biol Open*. 2:95–100.

Ke M-T, Fujimoto S, Imai T. 2013. SeeDB: a simple and morphology-preserving optical clearing agent for neuronal circuit reconstruction. *Nat Neurosci*. 16:1154–1161.

Ke M-T, Nakai Y, Fujimoto S, Takayama R, Yoshida S, Kitajima TS, Sato M, Imai T. 2016. Super-resolution mapping of neuronal circuitry with an index-optimized clearing agent. *Cell Rep*. 14:2718–2732.

Kebschull JM, Garcia da Silva P, Reid AP, Peikon ID, Albeanu DF, Zador AM. 2016. High-throughput mapping of single-neuron projections by sequencing of barcoded RNA. *Neuron*. 91:975–987.

LaMantia AS, Rakic P. 1990. Axon overproduction and elimination in the corpus callosum of the developing rhesus monkey. *J Neurosci*. 10:2156–2175.

Mao T, Kusefoglu D, Hooks BM, Huber D, Petreanu L, Svoboda K. 2011. Long-range neuronal circuits underlying the interaction between sensory and motor cortex. *Neuron*. 72: 111–123.

Marin-Padilla M. 1978. Dual origin of the mammalian neocortex and evolution of the cortical plate. *Anat Embryol*. 152:109–126.

Matsuda T, Cepko CL. 2007. Controlled expression of transgenes introduced by *in vivo* electroporation. *Proc Natl Acad Sci U S A*. 104:1027–1032.

Minamisawa G, Kwon SE, Chevée M, Brown SP, O'Connor DH. 2018. A non-canonical feedback circuit for rapid interactions between somatosensory cortices. *Cell Rep*. 23: 2718–2731.e6.

Mitchell BD, Macklis JD. 2005. Large-scale maintenance of dual projections by callosal and frontal cortical projection neurons in adult mice. *J Comp Neurol*. 482: 17–32.

Molyneaux BJ, Arlotta P, Fame RM, MacDonald JL, MacQuarrie KL, Macklis JD. 2009. Novel subtype-specific genes identify distinct subpopulations of callosal projection neurons. *J Neurosci*. 29:12343–12354.

Muzumdar MD, Tasic B, Miyamichi K, Li L, Luo L. 2007. A global double-fluorescent Cre reporter mouse. *Genesis*. 45: 593–605.

Niwa H, Yamamura K, Miyazaki J. 1991. Efficient selection for high-expression transfectants with a novel eukaryotic vector. *Gene*. 108:193–199.

O'Leary DDM, Stanfield BB, Cowan WM. 1981. Evidence that the early postnatal restriction of the cells of origin of the callosal projection is due to the elimination of axonal collaterals rather than to the death of neurons. *Dev Brain Res*. 1: 607–617.

Price DJ, Blakemore C. 1985. Regressive events in the postnatal development of association projections in the visual cortex. *Nature*. 316:721–724.

Ren S-Q, Li Z, Lin S, Bergami M, Shi S-H. 2019. Precise long-range microcircuit-to-microcircuit communication connects the frontal and sensory cortices in the mammalian brain. *Neuron*. 104:385–401.e3.

Rockel AJ, Hiorns RW, Powell TPS. 1980. The basic uniformity in structure of the neocortex. *Brain*. 103:221–244.

Rockland KS. 2013. Collateral branching of long-distance cortical projections in monkey. *J Comp Neurol*. 521:4112–4123.

Ruifrok AC, Johnston DA. 2001. Quantification of histochemical staining by color deconvolution. *Anal Quant Cytol Histol*. 23:291–299.

Saito K, Mizuguchi K, Horiike T, Dinh Duong TA, Shinmyo Y, Kawasaki H. 2019. Characterization of the inner and outer Fiber layers in the developing cerebral cortex of gyrencephalic ferrets. *Cereb Cortex*. 29:4303–4311.

Sakakibara A, Sato T, Ando R, Noguchi N, Masaoka M, Miyata T. 2014. Dynamics of centrosome translocation and microtubule organization in neocortical neurons during distinct modes of polarization. *Cereb Cortex*. 24: 1301–1310.

Scannell JW, Blakemore C, Young MP. 1995. Analysis of connectivity in the cat cerebral cortex. *J Neurosci*. 15: 1463–1483.

Schwartz ML, Goldman-Rakic PS. 1982. Single cortical neurones have axon collaterals to ipsilateral and contralateral cortex in fetal and adult primates. *Nature*. 299:154–155.

Sousa AMM, Meyer KA, Santpere G, Gulden FO, Sestan N. 2017. Evolution of the human nervous system function, structure, and development. *Cell*. 170:226–247.

Srivatsa S, Parthasarathy S, Molnár Z, Tarabykin V. 2015. Sip1 downstream effector *ninein* controls neocortical axonal growth, ipsilateral branching, and microtubule growth and stability. *Neuron*. 85:998–1012.

Takahashi N, Oertner TG, Hegemann P, Larkum ME. 2016. Active cortical dendrites modulate perception. *Science*. 354: 1587–1590.

Thompson A, Murphy D, Dell'Acqua F, Ecker C, McAlonan G, Howells H, Baron-Cohen S, Lai MC, Lombardo MV, the MRC AIMS Consortium, Catani M. 2017. Impaired communication between the motor and somatosensory homunculus is associated with poor manual dexterity in autism spectrum disorder. *Biol Psychiatry*. 81:211–219.

Velona T, Altounian M, Roque M, Hocine M, Bellon A, Briz CG, Salin P, Nieto M, Chauvet S, Mann F. 2019. PlexinD1 and Sema3E determine laminar positioning of heterotopically projecting callosal neurons. *Mol Cell Neurosci*. 100:103397.

Watakabe A, Kato S, Kobayashi K, Takaji M, Nakagami Y, Sadakane O, Ohtsuka M, Hioki H, Kaneko T, Okuno H, et al. 2012. Visualization of cortical projection neurons with retrograde TET-Off lentiviral vector. *PLoS ONE*. 7:e46157.

Watakabe A, Ohsawa S, Hashikawa T, Yamamori T. 2006. Binding and complementary expression patterns of semaphorin 3E and plexin D1 in the mature neocortices of mice and monkeys. *J Comp Neurol*. 499:258–273.

Watakabe A, Takaji M, Kato S, Kobayashi K, Mizukami H, Ozawa K, Ohsawa S, Matsui R, Watanabe D, Yamamori T. 2014. Simultaneous visualization of extrinsic and intrinsic axon collaterals in Golgi-like detail for mouse corticothalamic and corticocortical cells: a double viral infection method. *Front Neural Circuits*. 8:110.

Yagi H, Oka Y, Komada M, Xie M-J, Noguchi K, Sato M. 2016. Filamin A interacting protein plays a role in proper positioning of callosal projection neurons in the cortex. *Neurosci Lett*. 612:18–24.

Yamashita T, Pala A, Pedrido L, Kremer Y, Welker E, Petersen CCH. 2013. Membrane potential dynamics of neocortical projection neurons driving target-specific signals. *Neuron*. 80:1477–1490.

Yamashita T, Vavladeli A, Pala A, Galan K, Crochet S, Petersen SSA, Petersen CCH. 2018. Diverse long-range axonal projections of excitatory layer 2/3 neurons in mouse barrel cortex. *Front Neuroanat*. 12:33.